DOI: 10.21062/mft.2023.098 http://www.journalmt.com

Design of a Photoelectric Measuring Robot for Straightness of Deep/Blind Hole with Automatic Centering Function

Haifeng Zhao* (0000-0003-3292-5641)[1, 2]
[1]Department of Intelligent Manufacturing, Nanjing Information Vocational and Technical College, Nanjing 210023, China
[2]Jiangsu Provincial Robot Micro Servo Engineering Research Center, Nanjing 210023, China, *Corresponding author's E-mail: zhaohf@njcit.cn

In order to quickly measure the straightness parameters of the deep hole/blind hole axis, a robot for measuring the straightness of the deep hole/blind hole axis based on the photoelectric prin-ciple is designed. Using the linearity of the laser as a reference, the straightness of the inner hole can be detected through the function that the PSD sensor can accurately locate the position of the energy center of the light. By studying the relationship between the position of the light spot and the output voltage of the PSD device, the measurement model of the straightness of the deep hole axis is derived. During the measurement, the robot spiral driving mechanism moves back and forth inside the deep/blind hole, and the automatic centering mechanism realizes the precise positioning of the deep/blind hole axis. The laser fixed on the axis of the automatic centering mechanism can illuminate the PSD target to obtain the current position data of the deep/blind hole axis. Use the least square median method to eliminate the gross error of the obtained data, and the least square principle fitting can obtain the measurement results of the current axis straightness. In order to ensure the measurement accuracy, the measuring robot is calibrated by a standard ring gauge and used for the age of the pipe with an inner diameter of 135mm to obtain an error accuracy of less than 0.05 mm for the axis.

Keywords: Deep/blind hole, Straightness, Photoelectric measurement, Self-centering device, Position sensitive detector

1 Introduction

In modern industry, the deep/blind hole testing technology of precision instruments is the important factors that affect the quality of products. There are deep holes (holes with a length-diameter ratio greater than 5) or blind holes with different diameters in aircraft, ships, petroleum equipment and large medical devices. The detection technology of these holes directly affects the accuracy of the parts [1]. For deep hole/blind hole, its axis straightness is the basis for measuring other aperture parameters, and also the main index that affects the machining accuracy and performance of hole parts. At present, the inner diameter measurement technology of small and medium-sized hole parts is becoming more and more perfect. However, the measurement of large internal diameter, especially the internal diameter of large work pieces, still adopts the direct contact measurement methods such as the internal micrometer, the arm method, and the inductive strain gauge [2]. The precision of the direct contact measurement method is difficult to control, easy to be affected by human, and has poor stability. With the development of science and technology, some scholars have proposed non-contact measurement methods for deep hole diameter parameters. Kyofu Matsuda of Japan proposed the laser holography method, which uses a beam splitter to divide the laser into two beams, one of which falls beam falls on the holographic negative to form a target beam; after passing through the scattering plate, the beam falls and interferes with the front beam to form a hologram. During measurement, the straightness error value is obtained according to the change of interference fringe [3]. Yu Daguo used ultrasonic and reverse methods to measure the straightness of deep hole axis [4]. Getler MW invented an optical hole axis straightness indicator and successfully applied it to the field of weapon manufacturing [5]. The barrel straightness detection device proposed by Pont FDU is a detection technology that combines the optical imaging principle with the spiral micrometer [6]. Matsuzaki et al. discussed the influence of different number of guide block drills on the axis deflection of deep holes during machining [7]. P. Schalk used the image detection method to detect the straightness of the axis of the deep hole online [8]. Dawit H. Endrias of Canadian TS Technology Company proposed a method to accurately evaluate the regional spatial straightness from a set of coordinate measurement data points [9]. Akio Katsuki of Kyushu University in Japan developed a laser guidance device for drilling

guidance based on the interference principle of hole axis straightness detection [10]. Mindugas Jurevicius of the Dimis University of Technology in Vilnius and others have developed a device for accurately measuring straightness using non-contact optical mechanical methods [11]. The equipment calculates the straightness of the measured hole through the phase difference of the two signals received by the equipment. The straightness measurement of the axis of the deep-hole parts above mainly includes optical method, image method, ultrasonic detection method and other methods. Generally, the existing measurement methods have been applied to the measurement of the straightness of the axis of the deep hole/blind hole. However, the existing measurement methods need a large test space to arrange the equipment during the test process, and their test instruments are cumbersome and complex to operate, which cannot measure the straightness of the axis of the deep hole/blind hole parts quickly and accurately. Therefore, on the basis of the existing axis straightness test methods, it is of great significance to develop a small and precise automatic test instrument for rapid measurement of deep blind hole parts in complex environments.

In recent years, with the rapid development of sensor technology and robot technology, a large number of robots with different detection functions have emerged [12-14]. This research is based on robot technology and photoelectric measuring principle, and a high-precision blind hole straightness self-centering measuring robot based on PSD (position sensitive detector) is designed. The axial travel mechanism drives the axis self-centering device to move along the axial direction of the deep hole, and the laser emitted by the laser transmitter at the end of the axis centering mechanism projects on the PSD detection surface target. The signal processing system collects PSD spot position signals to form a sample set of the center of the cross section at different positions of the deep blind hole. The spatial linear equation of the actual hole center axis is obtained by data fitting, and the evaluation of the deep blind hole axis is completed by using the least square principle. The original contribution of this research is to combine robot technology with photoelectric measurement technology, and design an automatic measuring robot for deep/blind hole axis, which greatly reduces the layout environment of measuring optical instruments, and can quickly obtain the straightness parameters of part hole axis in a small range. By placing the measuring robot inside the inner hole of the deep hole to be measured, the sample set of axes at different positions of the deep/blind hole can be quickly obtained. The obtained data are fitted to obtain the spatial linear equation of the actual hole center axis, and the evaluation of the deep blind hole axis is completed using the least square principle.

2 Materials and Methods

2.1 Measuring principle

Photoelectric measurement technology refers to a physical phenomenon that light irradiates an object to cause the conductivity of the irradiated material to change. As a commonly used position sensitive device, PSD divides a circular photosensitive panel into four independent four-quadrant photodetectors [15] with equal area, same shape, symmetrical position and identical performance. When light sources in different positions il-luminate PSD panel, the spot areas projected on the four quadrants are different, and the voltage signals generated are also different. The voltage signals of each quadrant can be amplified and measured by the signal conditioning circuit. That is, the offsets and of the spot center in the and direction can be obtained [16,21].

Fig. 1 is the working principle diagram of PSD device. When the light illuminates the panel, the offsets and of the spot center in the and direction s are proportional to the incident spot areas of the four quadrants, which can be obtained by equation 1 and equation 2.

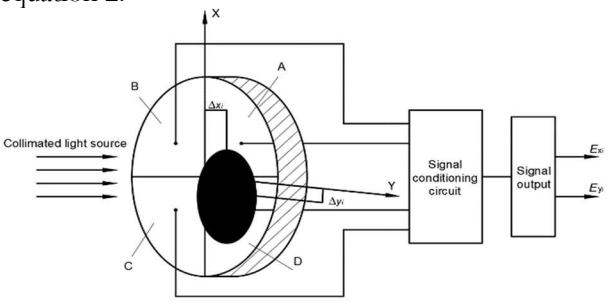

Fig. 1 *Working principle diagram of photodetector*

$$\Delta y_i = k_y \frac{S_A + S_B - (S_C + S_D)}{S_A + S_B + S_C + S_D} = k_y \frac{V_A + V_B - (V_C + V_D)}{V_A + V_B + V_C + V_D} = k_y E_{yi} \quad (1)$$

$$\Delta x_i = k_x \frac{S_A + S_D - (S_B + S_C)}{S_A + S_B + S_C + S_D} = k_x \frac{V_A + V_D - (V_B + V_C)}{V_A + V_B + V_C + V_D} = k_x E_{xi} \quad (2)$$

Where:

V_A , V_B, V_C and V_D... the signal voltages output by each quadrant of the detector [V],

S_A, S_B, S_C and S_D... the spot areas of each quadrant of the detector [M²],

E_{xi} and E_{yi} ... the potential difference signal output by the detector in the sum direction [V],

k_x and k_y ... which are obtained by calibration, Constants [-].

2.2 Design of measuring device

Based on the above photoelectric principle, the structure of a high-precision self-centering measuring robot for deep blind holes is shown in Fig. 2. It is mainly composed of seven parts: a spiral axial travelling mechanism I, an axis self-centering device II, a laser emitting device III and a PSD position detection panel IV, a PSD initial position zeroing device V, a data acquisition system VI and an upper computer processing system VII.

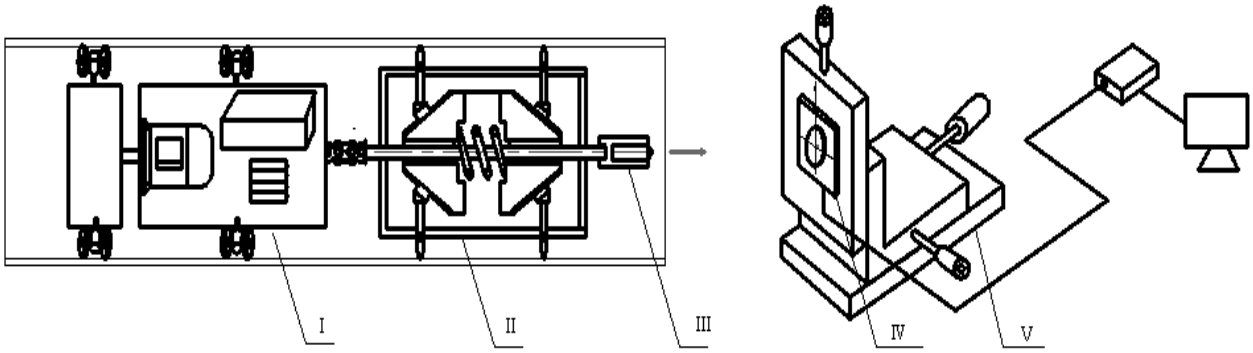

Fig. 2 *High-precision self-centering measuring robot for deep blind hole straightness*

2.2.1 Spiral axial traveling mechanism

The structure of the axial traveling mechanism is shown in Fig. 3, in which items 1-7 are lithium battery, guide wheel, stepping motor, rotor, spiral wheel, wire, Bluetooth module and control circuit.

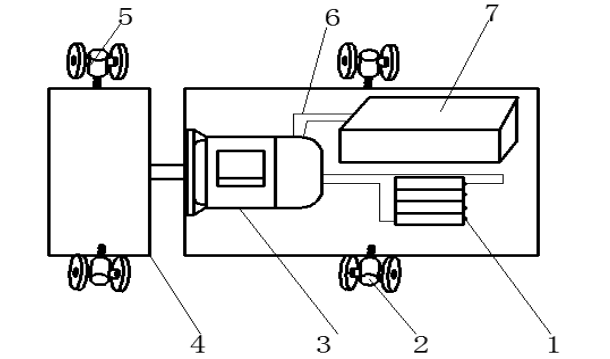

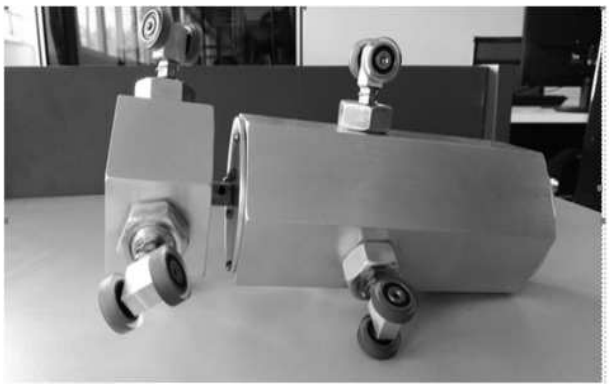

Fig. 3 *Structure diagram of spiral traveling mechanism*

When travelling axially, the hexagonal prism rotor 4 is driven by the stepping motor 3 to rotate circumferentially. Three groups of symmetrically arranged wheel frames are installed on the outer wall of the rotor, and two wheels are installed on each group of wheel frames. The rotation axis of the wheels and the axis of the rotor form a spiral angle (acute angle). The outer wall of the right hollow hexagonal prism is also provided with three groups of symmetrically arranged guide wheel frames. Each group of guide wheel frames is provided with two wheels, and the rotation axis of the wheels is perpendicular to the axis of the hexagonal prism. The wheel frame on the rotor and the wheel frame on the traveling wheel are floating bod-ies, and springs are respectively used to generate certain radial expansion and contraction, so that the wheels on the rotor wheel frame and all the wheels on the guide wheel frame are always attached to the inner wall of the pipeline to adapt to the change of the diameter of the pipeline within a certain range. Two parts of the rotor and the traveling wheel are connected through a shaft sleeve. When traveling, the controller, driver and Bluetooth module installed in the travelling wheel structure receive the control signal sent by the upper computer to drive the motor to rotate and thus use the spiral force to drive the device forward and backward. [20, 22]

2.2.2 Axis self-centering device

The axis self-centering device consists of two-way symmetrically distributed conical frus-tums 6 (with one on each side), sliding rails 7 (three on the right and three on the left) installed on the conical frustum and evenly distributed at 120 degrees, a sliding block 5 matched with the sliding rails, a leveling block 4, a fixed measuring rod 8, a replaceable measuring head 3, a built-in tension spring 10, a centering shaft 11, a ball sleeve 10, an integral sleeve 2 of the fixed axis centering device, and a detachable right end cover 1.

During measurement, 6 replaceable probes contact

with the cylinder wall. When the aper-ture becomes smaller, the probes drive the slider to squeeze the slide rail connected to the coni-cal frustum under the action of radial force and move to the middle along the aperture axis. At this time, the spring in the middle of the conical frustum is pressed. When the axial pressure and radial decomposition of the spring are balanced in the axial force component, the system tends to be stable, so that the local axial position of the current measured aperture can be accurately determined by the axial centering device. On the contrary, the spring expands and contracts, pushing the conical frustum to slide to both sides. The sliding table and the slide rail form a rel-ative movement, and the probes move outward along the radial direction until the contact force with the hole wall reaches a balance.

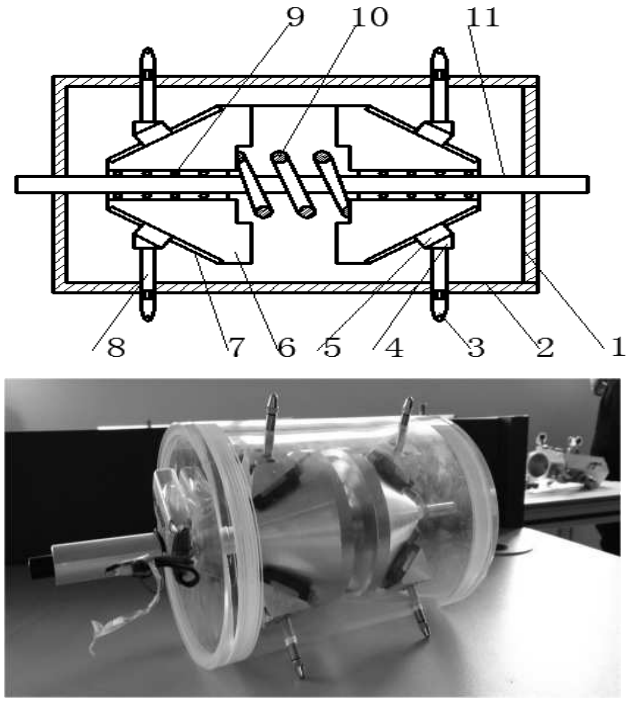

Fig. 4 *Structure diagram of axis self-centering device*

2.2.3 Laser emitting device

The laser emitting device consists of a laser sleeve 2 and a spot laser 1 fixed on the right side of the axis self-centering device, and the structure schematic diagram is shown in Fig. 5. When measuring, the laser 1 emits a spot parallel to the axis and irradiates the PSD panel sur-face [17].

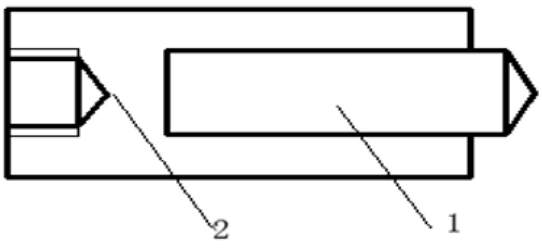

Fig. 5 *Structure diagram of laser emitting device*

2.2.4 PSD position detection panel

The measuring principle of photoelectric detection panel is shown in Fig. 1. During the measurement, when the incident light spot falls on different positions of the photosensitive sur-face of the device, each quadrant of the four-quadrant detector outputs electric signals with dif-ferent amplitudes. By calculating the amplitudes of these signals, the position of the center of the incident light spot on the photosensitive surface can be determined [18].

2.2.5 PSD initial position zeroing device

A typical X/Y/Z three-coordinate adjustment table is used to zero the initial position of the photodetector signal [19]. The schematic diagram of PSD initial position adjustment device is shown in Fig. 6, and its precision can reach 0.001mm. In Fig. 6, items 1-3 are Z coordinate adjustment knob, X coordinate adjustment knob and Y coordinate adjustment knob respectively.

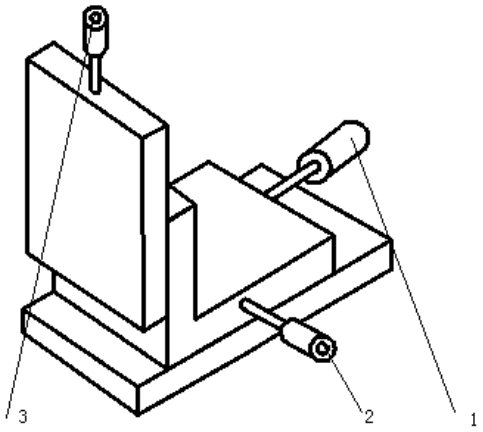

Fig. 6 *Schematic diagram of PSD position adjustment device*

2.2.6 Data acquisition system

The data acquisition system is responsible for the acquisition of photoelectric signals. The data acquisition module adopts the high-precision PSD position sensor signal acquisition and processing board produced by Shenzhen Daruixin Optoelectronics Technology Co., Ltd. The signal processor can provide RS232, RS485 and USB interfaces. The high-speed 18-bit AD chip is adopted, and high-precision PSD bias voltage is integrated inside. The processor can process photoelectric signals of one-dimensional and two-dimensional PSD position sensors and four-quadrant detectors.

2.2.7 Upper computer system

The upper computer system is responsible for signal calculation. It can display the Δx_i and Δy_i position deviation of the axis at any position relative to the initial measurement point in real time, and can display them in the form of two-dimensional axis.

2.3 Straightness model and evaluation

2.3.1 Physical model

For deep holes, straightness is the deviation between the axis of the hole center and the measured coordinates of the hole center in the ideal state, and its physical model can be shown in Fig. 7.

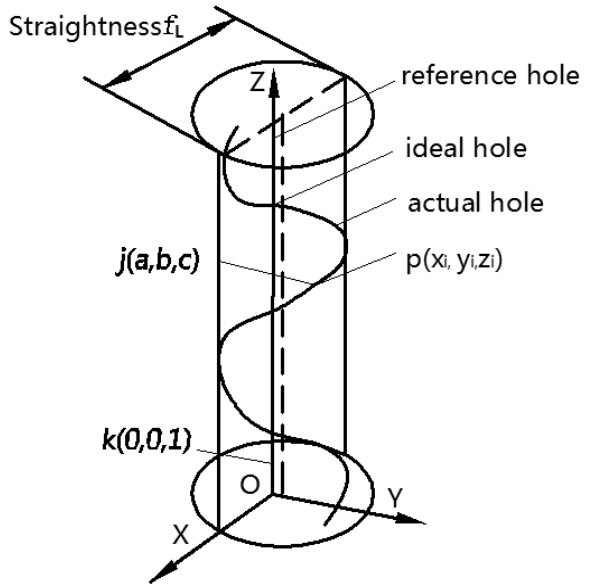

Fig. 7 *Spatial straightness evaluation model*

Wherein, $O_i(0,0,1)$ refers to the reference hole center direction vector; $M_i(X_i, Y_i, Z_i)$ refers to the measured coordinates of hole center at different positions; $N_i(X_i, Y_i, Z_i)$ refers to the position coordinates of hole center in the ideal state.

When measuring, the incident light illuminates the detection panel, and the spot usually appears in the following 4 forms on the detection panel.

(a) M_i coincides with N_i

At this time, the center of the spot coincides with the axis of the hole center in the ideal state. The center coordinates are (X, Y, Z_i), and the displacement change of the spot center on the photosensitive panel is 0. The spot projection is shown in Figure 8, and the spot equation is as follows.

$$x^2 + y^2 = r^2 \tag{3}$$

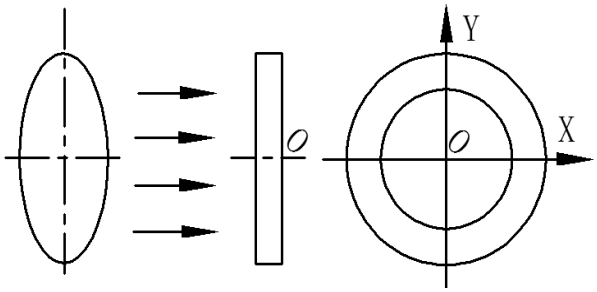

Fig. 8 *Initial spot shape and position*

(b) M_i is parallel to the N_i direction vector

At this time, the spot center deviates from the ideal hole center axis, and the spot center coordinates become(X, Y, Z_i). As shown in Fig. 9, the spot projection is still circular, and its equation becomes:

$$(x^2 - x_i^2) + (y^2 - y_i^2) = r^2 \tag{4}$$

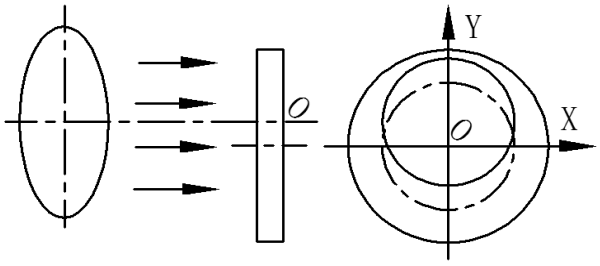

Fig. 9 *The photosensitive panel shifts*

Among it, X_i and Y_i can be obtained by the two equations (1) and (2).

(c) The center of the light spot crosses the ideal hole center coordinate and intersects with the direction vector.

At this time, the spot center coincides with the ideal hole center coordinates, and the spot center coordinates are still(X, Y, Z_i). As shown in Fig. 10, the spot projection is an ellipse with the center passing through the ideal hole center axis.

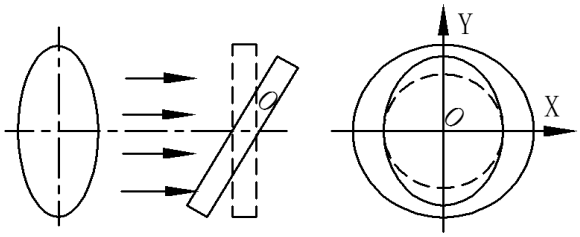

Fig. 10 *The photosensitive panel rotates*

(d) The center of the light spot deviates from the axis of the ideal hole center, and M_i intersects with theN_i direction vector.

At this time, as shown in Fig. 11, the spot projection is an ellipse deviating from the ideal hole center axis.

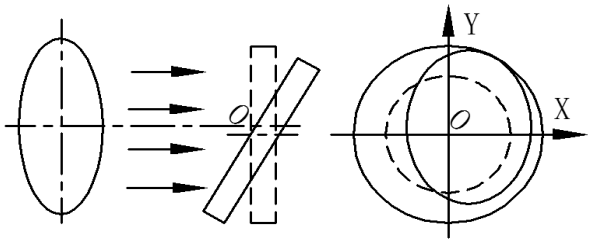

Fig. 11 *The photosensitive panel translates and rotates*

2.3.2 Least square evaluation

As this design adopts the external plate target measurement structure and its axis can be adjusted by the self-centering mechanism, the spot only presents shapes 1 and 2 on the detection panel, and the shape 1 is a special case of ideal state. Based on this, the designed mathematical model can be uniquely determined by the shape 2, which greatly optimizes the measurement model of deep hole straightness.

In shape 2, the sample space of the displacement change $M_i(X_i, Y_i, Z_i)$ of the spot center can be measured by the axial feed of the robot, with $i \in (1,2,3,\cdots,k)$. The sample $M_i(X_i, Y_i, Z_i)$ is the coordinate data of the center of the current cross section, and its measurement basis is based on the preset centering coordinates $O_i(A_i, B_i, Z_i)$of the measuring device. It is not necessarily the best evaluation of the overall center of the cross section, but it has the following relationship with the measured sample:

$$d_i^2 = (x_i - A_i)^2 + (y_i - B_i)^2 \tag{5}$$

Wherein, d_i is the distance from (X_i, Y_i) to the center of the circle. $i \in (1,2,3,\cdots,m-1)$.

The circle curve is fitted according to the least square method. The absolute value of the deviation between the measured sample point (X_i, Y_i) and the fitted circle is required to be the smallest. Let:

$$\partial_i = d_i^2 - R_i^2 = (x_i - A_i)^2 + (y_i - B_i)^2 - R^2 \tag{6}$$

After conversion of the above equation:

$$\partial_i = x_i^2 + y_i^2 + ax_i + by_i + c \tag{7}$$

In the above equation:$a = -2A; b = -2B; c = A_i^2 + B_i^2 - R_i^2$

When $M_i(a,b,c) = \partial_i^2 = \sum[x_i^2 + y_i^2 + ax_i + bx_i + c]^2$is the smallest, it is the least square fitting. At this point,

$$\begin{cases} \dfrac{\partial M(a,b,c)}{\partial a} = \sum 2(x_i^2 + y_i^2 + ax_i + by_i + c)x_i = 0 \\ \dfrac{\partial M(a,b,c)}{\partial a} = \sum 2(x_i^2 + y_i^2 + ax_i + by_i + c)y_i = 0 \\ \dfrac{\partial M(a,b,c)}{\partial a} = \sum 2(x_i^2 + y_i^2 + ax_i + by_i + c)z_i = 0 \end{cases} \tag{8}$$

Based on the above simultaneous equations, the center coordinates $O_i(A_i, B_i)$ and radius parameter $R_i$of the current section M_i can be obtained.

2.4 Error analysis and calibration of measuring robot

In the experimental test, due to the influence of the machining precision of the robot positioning mechanism and the testing environment, the system can't locate the pipeline axis completely and accurately, which will bring the system testing error. The essence of testing is to obtain the accurate parameters of the machine or structure, so it is necessary to analyze the error of the instrument and calibrate it.

2.4.1 Error of centering deicers

The centering device is mainly composed of mandrel, bearing, frustum, slide rail, probe fixing block, spring, fixed measuring rod, replaceable probe, mounting sleeve and other parts. Due to the processing reasons, the mandrel's own error is within the range of $\triangle_1$=0.01mm after calibration. The bearing is a standard component. Its diameter error is $\triangle_2$=0.02mm by lookup.

The cone is a machined piece. Its diameter error after machining and calibration is $\triangle_3$ = 0.01mm. The slide rail and slide block are precision linear slide blocks. Their precision is $\triangle_4$=0.007mm mm by lookup. The radial error of the work piece of the probe fixing block is $\triangle_5$=0.01mm. The fixed measuring rod and probe are standard parts, and the estimated error is $\triangle_6$=0.02mm. Therefore, the total radial error of the centering mechanism is $\triangle_{Total}=(\triangle_1+\triangle_2+\triangle_3+\triangle_4+\triangle_5+\triangle_6)/2$=0.0435mm.

2.4.2 Test error of laser measuring device

As a commonly used position sensitive device, PSD can measure the position of the incident spot center on the photosensitive surface with a precision of 0.001mm by calculating the amplitude of the laser signal.

2.4.3 Overall error

When measuring, the main precision of the measuring device depends on the precision of the centering device, and the precision of the centering device is mainly determined by the machining precision of each component. If high-precision machine tools are used for machining, the accumulated error of the components can be appropriately reduced. According to the above analysis, the overall measurement error of this axis measuring robot is less than 0.05mm.

2.4.4 Verification

To verify the errors caused by the design and processing of the instrument, the project has designed an experimental verification scheme. The specific experimental steps and scheme are as follows:

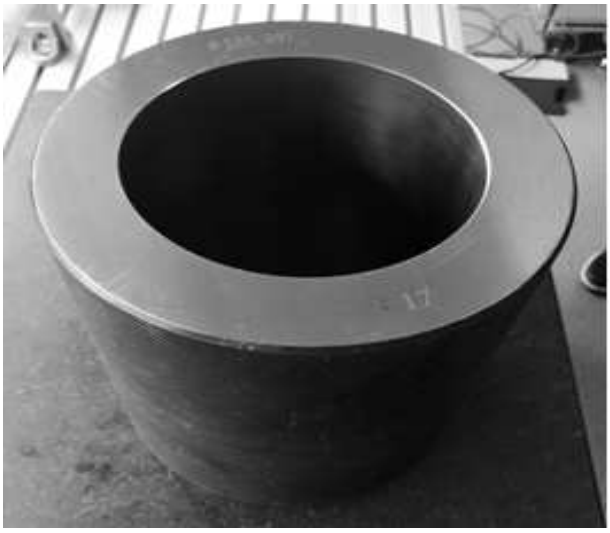

Fig. 12 *Professional measuring tool*

a) Design and order a professional measuring tool with a basic size of Φ134.997mm, a length of 200mm and a precision of 0.002 with the assistance of a professional measuring tool company, as shown in Fig. 12.

b) Build a calibration working environment, select a test plate with the precision of level 0, place the centering detection mechanism in the standard gauge, and test the data of different sections and different positions within 200mm. The calibration process is shown in Fig. 13.

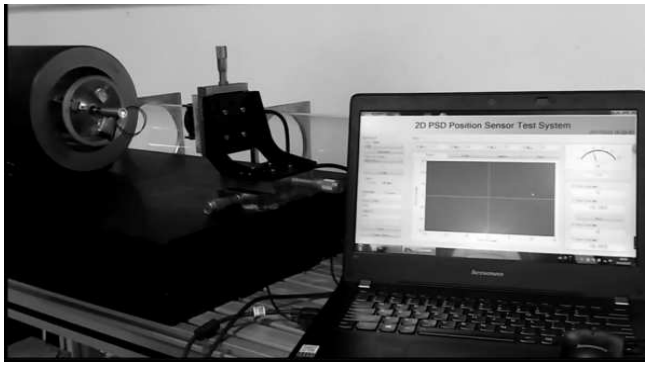

Fig. 13 *Field diagram of instrument calibration*

c) Carry out data test, complete data analysis, and draw verification conclusion. The veri-fication data are shown in Tab. 1.

Tab. 1 *Check 10-point data*

No.	X coordinate (mm)	Y coordinate (mm)	Center position offset (mm)
1	0	0	0
2	0.015	0.019	0.024
3	0.23	0.034	0.041
4	0.032	0.027	0.042
5	0.015	0.019	0.024
6	0.021	0.023	0.031
7	0.01	0.026	0.028
8	0.012	0.02	0.023
9	0.015	0.019	0.024
10	0.021	0.023	0.031

It can be seen from the analysis of data of ten different positions in the above test that the maximum variation of the diameter measured by the instrument is 0.042mm within the axial range, which does not exceed the error range of the instrument. Research manuscripts reporting large datasets that are deposited in a publicly available database should specify where the data have been deposited and provide the relevant accession numbers. If the accession numbers have not yet been obtained at the time of submission, please state that they will be provided during review. They must be provided prior to publication. Interventionary studies involving animals or humans, and other studies that require ethical approval, must list the authority that provided approval and the corresponding ethical approval code.

3 Discussion of results

In this paper, the PVC pipe with an inner diameter of 135mm and a length of 1000mm is measured by the measuring system. When measuring, the data acquisition card is connected with the upper computer, and the appropriate port is selected. The baud rate of signal transmission is 9600 B/s. Fig. 14 shows the measurement at the test site.

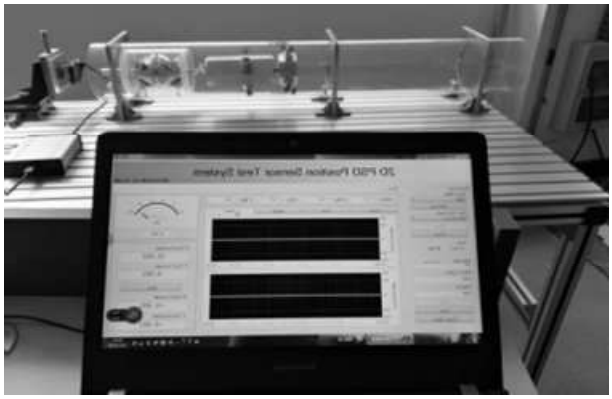

Fig. 14 *Measurement at test site*

When measuring, the relative measurement method is adopted. Therefore, the first step of measurement is the zeroing of the initial position. At this time, set the measuring robot to the initial position of the measured pipeline, adjust the PSD position adjusting device, and place the laser emitting spot in the center of the PSD panel, as shown in Fig. 15.

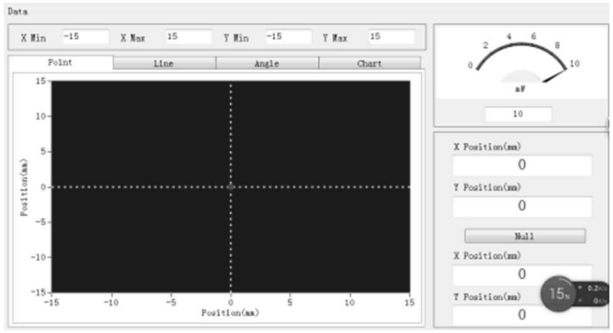

Fig. 15 *Schematic diagram of test zeroing*

After the zeroing is completed, the control end sends a forward signal, and the Bluetooth receiving module of the deep-hole traveling robot receives the signal to drive the device forward along the pipeline axis. At this time, the self-centering device will achieve self-balancing along with the change of the cross-section shape of the pipeline in the process of advancing, and the light spot emitted by the laser transmitter fixed at the rear end of the axis of the balancing device will automatically project on the four-quadrant photoelectric panel. The data acquisition device will collect and record the real-time pipeline axis position data, upload it to the upper computer and display it in the test software in real time. The test interface is shown in Fig. 16.

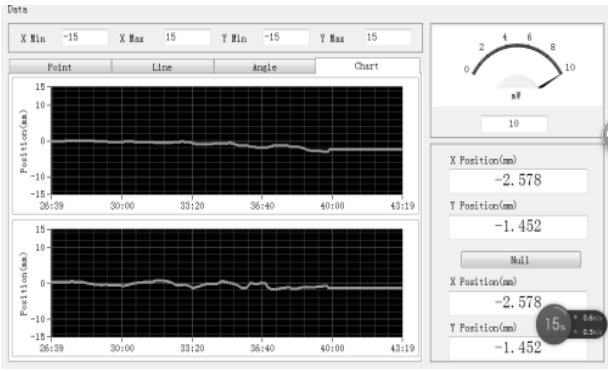

Fig. 16 *Schematic diagram of test zeroing*

During the test, due to the high sampling frequency and large volume of real-time recorded data, the data of different positions of the pipeline are selected and recorded as follows, as shown in Tab. 2.

Tab. 2 *Experimental data 1 of 135mm-diameter pipeline measured by mechanism*

X_1 Position (mm)	**Y_1 Position (mm)**	**S1 (mm)**
0	0	0
0.24	-0.058	0.247
0.24	-0.054	0.246
0.24	-0.054	0.246
0.22	-0.039	0.223
0.741	0.32	0.807
1.32	0.092	1.323
1.432	0.199	1.446
1.549	0.32	1.582
2.76	-0.506	2.806
2.419	0.066	2.420
2.355	0.094	2.357
2.356	0.116	2.359
2.389	0.119	2.392
2.903	0.021	2.903
3.102	0	3.102
2.641	-0.005	2.641
3.067	-0.374	3.090

In Tab. 2, the X_1 Position and the Y_1 Position respectively represent the X and Y position deviation distance of axis relative to initial position at different positions of the interface.$S1$ indicates the radius deviation of the current section from the initial zero point. It can be seen from the experimental data 1 that there is a big difference between the left and right axes of the inner diameter of the pipeline, with the maximum value of 3.090mm. The broken line of the pipeline axis change is shown in Fig. 17. If $f_L = 2S1max$, then$f_L = 6.180mm$.

To verify the reliability of the test data, the pipeline is retested, and the data are recorded as shown in Tab. 3 below. The experimental data in Tab. 2 and Tab. 3 are basically the same, with the maximum value of 3.097mm. The broken line of pipeline axis change is shown in Fig. 18. If $f_L = 2S2max$, then $f_L = 6.194mm$.

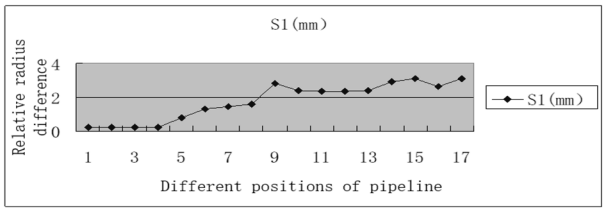

Fig. 17 *Broken line graph of pipeline axis error*

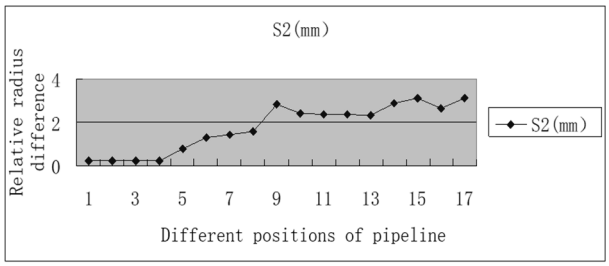

Fig. 18 *Broken line graph of pipeline axis error*

Tab. 3 *Experimental data 3 of 135mm-diameter pipeline measured by mechanism*

X_2 Position (mm)	Y_2 Position (mm)	S2 (mm)
0	0	0
0.239	-0.054	0.245
0.242	-0.053	0.248
0.240	-0.054	0.246
0.227	-0.039	0.230
0.731	0.302	0.796
1.320	0.092	1.323
1.435	0.199	1.449
1.552	0.319	1.584
2.775	-0.487	2.817
2.417	0.068	2.418
2.361	0.112	2.364
2.384	0.135	2.389
2.340	0.123	2.343
2.897	0.004	2.897
3.104	0.001	3.104
2.644	-0.009	2.644
3.073	-0.384	3.097

The two measurement results are compared, and the S1-S2 difference is taken. The broken line of repeated measurement error is shown in Fig. 19.

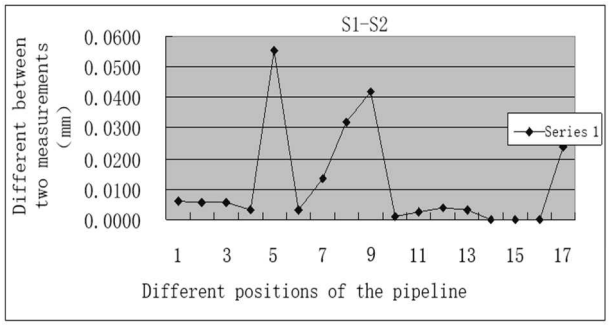

Fig. 19 *Broken line graph of repeated measurement error*

As can be seen from the above figure, the two measurement results are basically similar. The maximum repetitive error is in the middle position of the pipeline, and the error is less than 0.05mm. Compared with the existing methods, the axis straightness measurement robot designed in this paper can quickly measure the axis straightness parameters of part holes in a narrow space, which greatly reduces the time required for the layout and installation of other instruments. In the future, a sensor for detecting the characteristic defects of the inner wall surface can be added at the front end of the measuring device to better observe the inner wall of the deep-hole parts and provide a certain basis for the straightness measurement of the sampling section.

4 Conclusions

Based on the photoelectric principle, a PSD high-precision self-centering measuring robot for blind hole straightness is designed. By studying the relationship between the light spot posi-tion of PSD device and the output voltage and analyzing the change rule of measuring light spot, the straightness measurement model of deep hole inner diameter is deduced. The axial travel mechanism drives the axis self-centering device to move along the axial direction of the deep hole, and the laser transmitter at the end of the axis of the centering mechanism emits laser light to project on the photoelectric signal detection board target. The signal processing system col-lects the spot position signals to form a sample set of the center of the cross section of the deep blind hole at different positions. The spatial linear equation of the actual hole center axis is ob-tained by data fitting, and the evaluation of the deep blind hole axis is completed by using the least square principle. The gross error is eliminated by the least square median method, and the measurement results are fitted by the least square principle. The measurement system is cali-brated by the standard ring gauge, and it is used to measure a pipe with an inner diameter of 135 mm. The error of two measurements is less than 0.05 mm. The experimental results show that the measurement system has certain reliability.

Acknowledgement

This research was funded Supported by the major Project of Basic Science Research of Higher Education Insti-tutions in Jiangsu Province (2022KJA460012); The intelligent robot project of the Science and Technology De-velopment, Center of the Ministry of Education: the design of multifunctional inspection robot for underground pipelines based on multi-source in-formation fusion (2021JQR014) project. Author are grateful for Jiangsu Provincial Department of Education and Beijing Iron Man Robot Company.

References

[1] SHU, P.S. (2017). Research on Design and Test Method of Deep Hole Comprehensive Parameter Testing Device, *In: Tool Technology,* No. 6, pp.135-136.

[2] WANG, N.X. (2007). Design and application of deep hole straightness detection device, *In: Mechanical Design and Manufacturing,* No. 2, pp.12-13.

[3] JESCHKE, W. (1990). Digital close-range photogrammetry for surface measurement, *In: Proceedings of SPIE,* No. 1395, pp. 1058-1065.

[4] YU, D.G. (2016). Design of Deep-hole Straightness Measurement Device and Research for Its Algorithm, *In: Mehanical design and research,* Vol. 32, No.3, pp. 92-105.

[5] BIERMANN, D., IOVKOV, I. (2015). Investigations on the formation of straightness deviation in MQL deep-hole drilling of thin-walled aluminum components, *In: Production Engineering Research and Development,* Vol. 9, No. 4, pp.527-535.

[6] OKUD, K., YAMAGUCHI, T., YAMAAMOTO, T. (2014). A Study on Straightness of Deep Hole in Small-diameter drilling of Stainless Steel, *In: Advanced Materials Research,* No. 1017, pp.344-349.

[7] MATSUZAKI, K., RYU, T., SUEOK, A. (2015).Theoretical and experimental study on rifling mark generating phenomena in BTA deep hole drilling process, *In: International Journal of Machine Tools Manufacture,* Vol.88, pp.194-205.

[8] SCHALK, P,. OFNER, R,. LEARY, O. (2007). Pipe eccentricity measurement using laser triangulation, *In: Image and Vision Computing,* Vol. 25, No.7, pp.194-196.

[9] DAWIT, H., ENDRIA, S. (2012). A combinatorial optimization approach for evaluating minimum-zone spatial straightness errors, *In: Measurement,* Vol. 45, No.5, pp: 1170-1179.

[10] AKIO, K., TAKAO, S., HIROSHI, M. (2020). Development of a laser-guiding-type deep small-sized hole-measurement system: Measurement accuracy, *In: Precision Engineering,* Vol. 63, No.5, pp: 18-32.

[11] MINDAUGAS, J., JONAS, S. (2013). Robertas Urbanavicius. Accuracy evaluation of two-dimensional straightness measurement method based on optical meter, *In: Measurement,* Vol. 46, No. 2, pp.960-963.

[12] YIN, Y. (2019). Mult-sensor integration method of high-precision pipeline measurement robot, *In: Electronic Measurement Technology,* No. 02, pp. 23-27.

[13] SONG, C. (2022). Development and testing of a muti-sensor measurement system for roundness and axis straightness errors of deep-hole parts, *In: Measurement,* Vol. 198, No. 7, pp.1-26.

[14] CHEN, B.Y. (2015). Laser straightness interferometer system with rotational error compensation and simultaneous measurement

of six degrees of freedom error parameters, *In: Optics Express,* Vol. 23, No. 7, pp. 9052-9073.

[15] Zatočilová, A. (2016). Image-based measurement of the dimensions and of the axis straightness of hot forgings, *In: Measurement,* Vol. 94, No. 12, pp. 254-264.

[16] Zheng, F.J. (2019). A method for simultaneously measuring 6DOF geometric motion errors of linear and rotary axes using lasers, *In: Sensors,* Vol. 19, No. 8, pp.1764-1773.

[17] LI, J. (2019). Method for simultaneously and directly measuring all six-DOF motion errors of a rotary axis, *In: Chinese Optics Letters,* Vol. 17, No. 1 pp: 011203.

[18] Li, X.Q. (2016). A Fast and in-Situ Measuring Method Using Laser Triangulation Sensors for the Parameters of the Connecting Rod, *In: Sensors,* Vol. 16, No. 10, pp. 1679-1786.

[19] RHINITHAA, P.T., SELVAKUMAR, P. (2018). Comparative study of roundness evaluation algorithms for coordinate measurement and form data, *In: Precision Engineering,* Vol. 51, No. 1, pp.458-467.

[20] NASIR, N.S., AB WAHAB, N., BIN SOFIAN, B., IZAMSHAH, R. & SASAHARA, H. (2021). Experimental Investigations Towards Hole Accuracy in Micro-drilling of Carbon Fibre Reinforced Polymer Material. *Manufacturing Technology*, 21, 381-6.

[21] ZHENG, Y., WU, Z. & MA, C. (2022). Structural Optimization of Small Diameter Deep Well Rescue Robot Based on Hyperworks-Optistruct. *Manufacturing Technology*, 22, 771-6.

[22] PELLEGRINI, G. & RAVASIO, C. (2022). Experimental Investigation on the Effects of the Geometry of Micro Hole on the EDM Drilling Process. *Manufacturing Technology*, 22, 455-60.